Applied Catalysis B: Environmental 220 (2018) 42–56

Contents lists available at ScienceDirect

Applied Catalysis B: Environmental

journal homepage: www.elsevier.com/locate/apcatb

Effects of concentration and microstructure of active phases on the selective hydrodesulfurization performance of sulfided $CoMo/Al_2O_3$ catalysts

Tingting Huang, Jundong Xu, Yu Fan *

State Key Laboratory of Heavy Oil Processing, China University of Petroleum, Beijing 102249, PR China

ARTICLE INFO

Article history:
Received 2 May 2017
Received in revised form 18 July 2017
Accepted 8 August 2017
Available online 12 August 2017

Keywords:
CoMo catalysts
Selective hydrodesulfurization
CoMoS phase
MoS_2 phase
Microstructure

ABSTRACT

This investigation offers new understanding regarding the nature of CoMoS and MoS_2 active phases coexisting on sulfided $CoMo/Al_2O_3$ catalysts for the selective hydrodesulfurization (HDS) of gasoline. Two series of the $CoMo/Al_2O_3$ catalysts with different ethylenediaminetetraacetic acid (EDTA)/Co molar ratios and the EDTA-containing $CoMo/Al_2O_3$ catalysts with different cobalt contents were prepared, and the properties of their active metal phases were systematically correlated with their HDS selectivities. It was found that a high concentration of CoMoS phases improves the HDS activity of the sulfided $CoMo/Al_2O_3$ catalysts but that a high concentration of MoS_2 phases enhances the olefin hydrogenation (OHYD) activity of these catalysts. From the perspective of microstructure, it was evident that the thiophene HDS reaction occurs primarily at the edge of CoMoS active phases and that the OHYD reaction occurs mainly at the corner of MoS_2 active phases. These understandings shed light on the development of highly selective HDS catalysts.

1. Introduction

With increasingly stringent environmental legislations on vehicle emission pollution, the limitations on the sulfur content in vehicle fuel standards are becoming stricter [1,2]. How to effectively reduce the sulfur content in gasoline has become a significant research topic for clean gasoline production [3–5]. Fluid catalytic cracking (FCC) gasoline, which is the primary component of the gasoline pool, is the major sulfur contributor (more than 90%) in commercial gasoline; therefore, the desulfurization of commercial gasoline is focused on the sulfur reduction of FCC gasoline [4]. In the past years, many efforts have been made to determine the sulfur distribution in FCC gasoline [6,7], and the results showed that the most important class of sulfur-containing compounds present in FCC gasoline is composed of thiophene and its light alkyl derivatives in addition to benzothiophene. Yin et al. reported that thiophene sulfur takes a large share of the total sulfur content in FCC gasoline (more than 60 wt.%) [8]. However, there are no dibenzothiophene (DBT) and dimethyldibenzothiophene (DMDBT) derivatives in gasoline [4]. Although the refractory sulfur-containing compounds (such as DBT and DMDBT) with steric hindrance have low reactivity [9], thiophene with no steric hindrance has high reactivity. Because the main sulfur-containing compounds in FCC gasoline are thiophenic compounds, thiophene was selected as the representative sulfur-containing compound to investigate the activity and selectivity of the prepared catalysts for FCC gasoline desulfurization. It is widely accepted that hydrodesulfurization (HDS) is one of the most important technologies for gasoline desulfurization. It is imperative to develop a highly selective HDS process to remove the maximum amount of sulfur impurities and minimize olefin hydrogenation (OHYD) to maintain a high gasoline octane number [10,11]. Therefore, hydrotreating catalysts that have both high HDS activity and low olefin saturation activity are highly desired [12].

The HDS activity and the olefin saturation of hydrotreating catalysts are closely related to the properties of their active phases [13]; therefore, it is crucial to clarify the structure and location of the active phases of hydrotreating catalysts for specific reactions, which can provide a theoretical basis for the development of new catalysts to better tune the HDS/OHYD selectivity in the HDS process. The structures of the catalytic phases involved in HDS and OHYD reactions have been widely and thoroughly studied in recent decades [14–16]. The active phase in sulfide catalysts is mainly explained by the Co-Mo-S phase model [14]. In the Co-Mo-S phase model developed by Topsøe et al. [15], highly dispersed MoS_2 slabs were decorated by Co atoms at the edge and corner

* Corresponding author.
E-mail address: fanyu@cup.edu.cn (Y. Fan).

http://dx.doi.org/10.1016/j.apcatb.2017.08.029
0926-3373/

sites of the MoS_2 slabs. Miller et al. considered that HDS and OHYD reactions occurred in the identical type of active phases in sulfide catalysts [16]. However, on account of density functional theory (DFT) calculations, the corner sites of active phases are more conducive thermodynamically to the adsorption and dissociation of molecular H_2 [17]; furthermore, it is speculated that the corner sites of MoS_2 phases could account for the OHYD reaction and that the edge sites of MoS_2 phases could be responsible for the HDS reaction [18]. Li et al. reported that the HDS selectivity in the hydrogenation of thiophene and 1-hexene correlated linearly with the length of MoS_2 slabs; longer slabs were favorable for the improvement of HDS selectivity [19]. Nikulshin et al. tested the HDS reactivity of thiophene and the hydrogenation reactivity of 1-hexene over a series of $CoMo/Al_2O_3$ [20]. The results showed that the HDS selectivity correlated linearly with the edge-to-corner ratio of CoMoS phases.

Based on these arguments, the HDS/OHYD selectivity of sulfide catalysts is closely related to the concentration and microstructure of the active phases in sulfide catalysts, but it is under debate how the active phases in sulfide catalysts improve the HDS/OHYD selectivity of sulfide catalysts. To clarify the above arguments, in this investigation, the concentration and microstructure of MoS_2 and CoMoS active phases in sulfided $CoMo/Al_2O_3$ catalysts were finely adjusted by changing the amount of ethylenediaminetetraacetic acid (EDTA) and the content of cobalt. The active phase concentrations of the series of sulfided $CoMo/Al_2O_3$ catalysts were determined according to the CO-adsorbed infrared (CO-IR) spectra, and the effect of active phase concentration on the HDS reactivity of thiophene and the hydrogenation reactivity of 1-pentene were clarified. According to CO-IR, high resolution transmission electron microscopy (HRTEM) and X-ray photoelectron spectroscopy (XPS) measurements, the effects of microstructure of active phases over sulfided $CoMo/Al_2O_3$ catalysts on the HDS activity and selectivity of sulfided $CoMo/Al_2O_3$ catalysts were discussed. Based on the results obtained, a novel relationship between the nature of active phases over sulfided $CoMo/Al_2O_3$ catalysts and selective HDS performance was established.

2. Experimental

2.1. Catalyst preparation

The catalysts were prepared by incipient wetness impregnation of a shaped Al_2O_3 support (Shandong Alumina Plant, P.R. China).

A series of Co-Mo-EDTA/Al_2O_3 catalysts containing 3.0 wt.% CoO, 13.0 wt.% MoO_3 and different amounts of EDTA (1.0, 1.2, 1.4 and 1.6 molar ratio of EDTA/Co) were prepared as follows: EDTA was first dissolved in a concentrated NH_4OH solution, and aqueous cobalt nitrate ($Co(NO_3)_2{\cdot}6H_2O$) was added after EDTA dissolution; then, the required amount of a basic solution of ammonium heptamolybdate-4-hydrate (AHM) was added. The resulting solution was used to impregnate the shaped alumina support, and the impregnated product was dried in air at ambient temperature overnight and dried at 120 °C for 6 h. Before sulfidation, calcination was omitted to avoid the decomposition of EDTA. These catalysts are designated 3.0CoMo-xEDTA, where x is the molar ratio of EDTA/Co (1.0–1.6).

Another series of Co-Mo-EDTA/Al_2O_3 catalysts contained 13.0 wt.% MoO_3, different amounts of CoO (1.0, 2.0, 3.0 and 4.0 wt.%) and different amounts of EDTA with the molar ratio of EDTA/Co = 1.4. This series of catalysts was prepared using the same steps as those for Catalyst 3.0CoMo-xEDTA according to the required loadings. These catalysts are designated yCoMo-1.4EDTA, where y corresponds to the loading of CoO (1.0–4.0 wt.%).

The Co-Mo/Al_2O_3 catalyst prepared without EDTA involved the following steps: the required amounts of AHM and $Co(NO_3)_2{\cdot}6H_2O$ were dissolved in distilled water, and the shaped Al_2O_3 support was impregnated with the resulting solution. The impregnated product was dried in air at ambient temperature overnight; the precursor was dried at 120 °C for 6 h and calcined at 550 °C for 4 h [21,22]. The prepared catalyst is denoted as 3.0CoMo.

The compositions of all the catalysts are displayed in Table 1.

2.2. Catalyst characterization

2.2.1. CO-IR

The concentrations of the CoMoS and MoS_2 phases on the catalysts were characterized by a Nicolet 6700 equipped with a MCT detector. The catalysts were ground and pressed into self-supported wafers, which were mounted in the FT-IR cell. After purging with Ar for 2 h, the catalysts were sulfided in situ at 360 °C for 2 h in a flow of 15% H_2S/H_2 and then flushed with Ar at 360 °C for 1 h. After cooling to room temperature in a pure Ar flow, the cell was evacuated to 10^{-3} Pa. The sulfided catalysts were heated from room temperature to 350 °C and maintained at that temperature for 1 h. Then, the catalysts were cooled to −196 °C before CO introduction, and a reference spectrum of the sulfided catalyst was recorded. Finally, a spectrum was obtained at 133 Pa of CO in equilibrium with the sulfided catalyst.

2.2.2. HRTEM

The morphology of the active phases on sulfided catalysts was characterized by a FEI Tecnai G2 F20 microscope with a 0.14 nm lattice-fringe resolution. The samples used for HRTEM measurement were dispersed on a carbon-coated copper grids; 20 representative images were obtained for each sample and more than 500 MoS_2 slabs were measured for each sample. According to the literature [23], the average length ($\bar{L}$) and the average stacking number ($\bar{N}$) of MoS_2 slabs are expressed by the following equation:

$$\bar{L}(\bar{N}) = \frac{\sum_{i=1}^{n} x_i M_i}{\sum_{i=1}^{n} x_i} \quad (1)$$

where x_i is the number of MoS_2 slabs possessing L_i length or N_i number of layers and M_i is the length or layer number of MoS_2 slabs in each stack.

MoS_2 dispersion (D) is expressed by the following equation [20]:

$$D = \frac{Mo_e + Mo_c}{Mo_T} = \frac{\sum_{i=1}^{t} \left(6n_i - 6\right)}{\sum_{i=1}^{t} \left(3n_i^2 - 3n_i + 1\right)} \quad (2)$$

where Mo_e and Mo_c are the number of Mo atoms at the edge and corner sites; Mo_T is the total number of Mo atoms; n_i is the number of Mo atoms along one side of the MoS_2 slab, as calculated by its length ($L = 3.2(2n_i - 1)\mathring{A}$); and t is the total number of slabs in the TEM images.

The edge-to-corner ratio of a MoS_2 slab $\left(f_e/f_c\right)_{Mo}$ was determined by the equation [19]:

$$(f_e/f_c)_{Mo} = \frac{10 \times \bar{L}/3.2 - 3}{2} \quad (3)$$

2.2.3. XPS

XPS analysis of the sulfided catalysts was conducted on an ESCA Lab 250 electron spectrometer (VG Scientific) equipped with an Al

Table 1
Compositions of the prepared catalysts before sulfidation.

Catalyst	CoO (wt.%)	MoO_3 (wt.%)	Co/(Co + Mo) molar ratio	EDTA/Co molar ratio
3.0CoMo	3.0	13.0	0.31	0
3.0CoMo-1.0EDTA	3.0	13.0	0.31	1.0
3.0CoMo-1.2EDTA	3.0	13.0	0.31	1.2
3.0CoMo-1.4EDTA	3.0	13.0	0.31	1.4
3.0CoMo-1.6EDTA	3.0	13.0	0.31	1.6
1.0CoMo-1.4EDTA	1.0	13.0	0.13	1.4
2.0CoMo-1.4EDTA	2.0	13.0	0.23	1.4
4.0CoMo-1.4EDTA	4.0	13.0	0.37	1.4

Kα radiation with an energy resolution of 0.4 eV. The binding energy of Al2p peak (74.5 eV) was set as an internal standard. Before measurement, the sulfided samples were protected in cyclohexane to avoid oxidation. The sulfided catalyst was mounted on a holder. The collected spectra were analyzed using XPSPEAK version 4.1 software [24]. The decompositions of the Mo3d and Co2p XPS spectra were completed using the mixed Gaussian-Lorentzian function [25,26].

The absolute content of species j $C(j)_T$, the effective Co content of the CoMoS species C_{CoMoS}, the effective Mo content in MoS_2 phase C_{MoS_2}, the promoter ratio in the slab of CoMoS phase $(Co/Mo)_{slab}$, the promoter ratio in the slab corner and edge of CoMoS phase $(Co/Mo)_{e+c}$ and the edge-to-corner ratio of the CoMoS slab $(f_e/f_c)_{CoMo}$ were determined according to the method reported in the literature [27].

$$C(j)_T(\%) = \frac{A_j/S_j}{\sum i = 1\ldots nA_i/S_i} \times 100 \quad (4)$$

$$C_{CoMoS} = \frac{A_{CoMoS}}{A_{CoMoS}+A_{Co_9S_8}+A_{Co^{2+}}} \times C(Co)_T \quad (5)$$

$$C_{MoS_2} = \frac{A_{MoS_2}}{A_{MoS_2}+A_{MoO_xS_y}+A_{MoO_3}} \times C(Mo)_T \quad (6)$$

$$(Co/Mo)_{slab} = \frac{C_{CoMoS}}{C_{MoS_2}} \quad (7)$$

$$\left(\frac{Co}{Mo}\right)_{e+c} = \frac{(Co/Mo)_{slab}}{Mo_e + Mo_c} \times Mo_T = \frac{(Co/Mo)_{slab}}{D} \quad (8)$$

$$\left(\frac{f_e}{f_c}\right)_{CoMo} = \left(\frac{f_e}{f_c}\right)_{Mo} \times \left(\frac{Co}{Mo}\right)_{e+c} \quad (9)$$

where A_i is the calculated area of species i (Co^{2+}, Co_9S_8, CoMoS, MoS_2, MoO_xS_y and MoO_3) and S_i is the sensitivity factor of the atom related to species i.

Assuming that the Co atoms are homogenously dispersed on the corner and edge positions of the MoS_2 slab [19,20,27], the amounts of CoMoS phases at the corner and edge sites ($C(CoMoS)_c$ and $C(CoMoS)_e$) are calculated from $(f_e/f_c)_{CoMo}$ and the total concentration of CoMoS phases (C(CoMoS)) obtained from the CO-IR characterization:

$$C(CoMoS)_c = \frac{1}{(f_e/f_c)_{CoMo} + 1} \times C(CoMoS) \quad (10)$$

where $(f_e/f_c)_{CoMo}$ is the edge-to-corner ratio of the CoMoS slab, $(f_e/f_c)_{CoMo} + 1$ is the ratio between the total amount of CoMoS phases and the amount of CoMoS phases at the corner sites, $\frac{1}{(f_e/f_c)_{CoMo}+1}$ is the ratio between the amount of CoMoS phases at the corner sites and the total amount of CoMoS phases, and $\frac{1}{(f_e/f_c)_{CoMo}+1} \times C(CoMoS)$ is the amount of CoMoS phases at the corner sites.

$$C(CoMoS)_e = \frac{(f_e/f_c)_{CoMo}}{(f_e/f_c)_{CoMo} + 1} \times C(CoMoS) \quad (11)$$

where $\frac{(f_e/f_c)_{CoMo}}{(f_e/f_c)_{CoMo}+1}$ is the ratio between the amount of CoMoS phases at the edge sites and the total amount of CoMoS phases, and $\frac{(f_e/f_c)_{CoMo}}{(f_e/f_c)_{CoMo}+1} \times C(CoMoS)$ is the amount of CoMoS phases at the edge sites.

The amounts of MoS_2 phases at the corner and edge sites ($C(MoS_2)_c$ and $C(MoS_2)_e$) are calculated using $(f_e/f_c)_{Mo}$ and the total concentration of MoS_2 phases ($C(MoS_2)$) obtained from the CO-IR characterization:

$$C(MoS_2)_c = \frac{1}{(f_e/f_c)_{Mo} + 1} \times C(MoS_2) \quad (12)$$

$$C(MoS_2)_e = \frac{(f_e/f_c)_{Mo}}{(f_e/f_c)_{Mo} + 1} \times C(MoS_2) \quad (13)$$

The ratio between the amount of MoS_2 atoms on the corner and the amount of CoMoS and MoS_2 atoms on the corner ($r(MoS_2)_c$) as well as the ratio between the amount of CoMoS atoms on the edge and the amount of CoMoS and MoS_2 atoms on the edge ($r(CoMoS)_e$) was expressed by the following equations:

$$r(MoS_2)_c = \frac{C(MoS_2)_c}{C(MoS_2)_c + C(CoMoS)_c} \quad (14)$$

$$r(CoMoS)_e = \frac{C(CoMoS)_e}{C(MoS_2)_e + (CoMoS)_e} \quad (15)$$

2.2.4. Elemental analyses

X-ray fluorescence spectroscopy (XRF) analyses of the catalysts were carried out on an AxiosmAX instrument to measure the Co, Mo and Al contents. The carbon contents of the as-prepared catalysts were determined on a Leco CS600 carbon analyzer.

2.3. Catalytic assessment

The catalytic activities of the catalysts were evaluated in a fixed-bed micro-reactor with a loading of 0.6 g, using a mixture of thiophene (500 μg/g S), 1-pentene (30 wt.%) and *n*-heptane (as solvent) as a model compound. The reactions were carried out at 290 °C, 1.5 MPa, liquid hourly space velocity (LHSV) 3.5 h^{-1}, and a H_2/oil ratio of 300 (v/v). Before the assessments, the catalysts were pre-sulfurized at 360 °C for 6 h with 3 wt.% carbon disulfide (CS_2) in *n*-heptane. The hydrocarbon compositions of products were analyzed using an Agilent 1790 gas chromatograph (GC) installed with a flame ionization detector (FID) and an HP-PONA capillary column (50 m × 0.2 mm). The total sulfur contents of the feedstock and products were analyzed with an analytic Jena Multi EA 5000 (Germany) instrument using the pyrolysis method, in accordance with the international standard (ASTM D5453).

The conversion of total sulfur (HDS) and the conversion of olefin hydrogenation (OHYD) were calculated as follows [28]:

$$HDS(\%) = \frac{S_F - S_P S_F}{} \quad (16)$$

$$OHYD(\%) = \frac{O_F - O_P}{O_F} \quad (17)$$

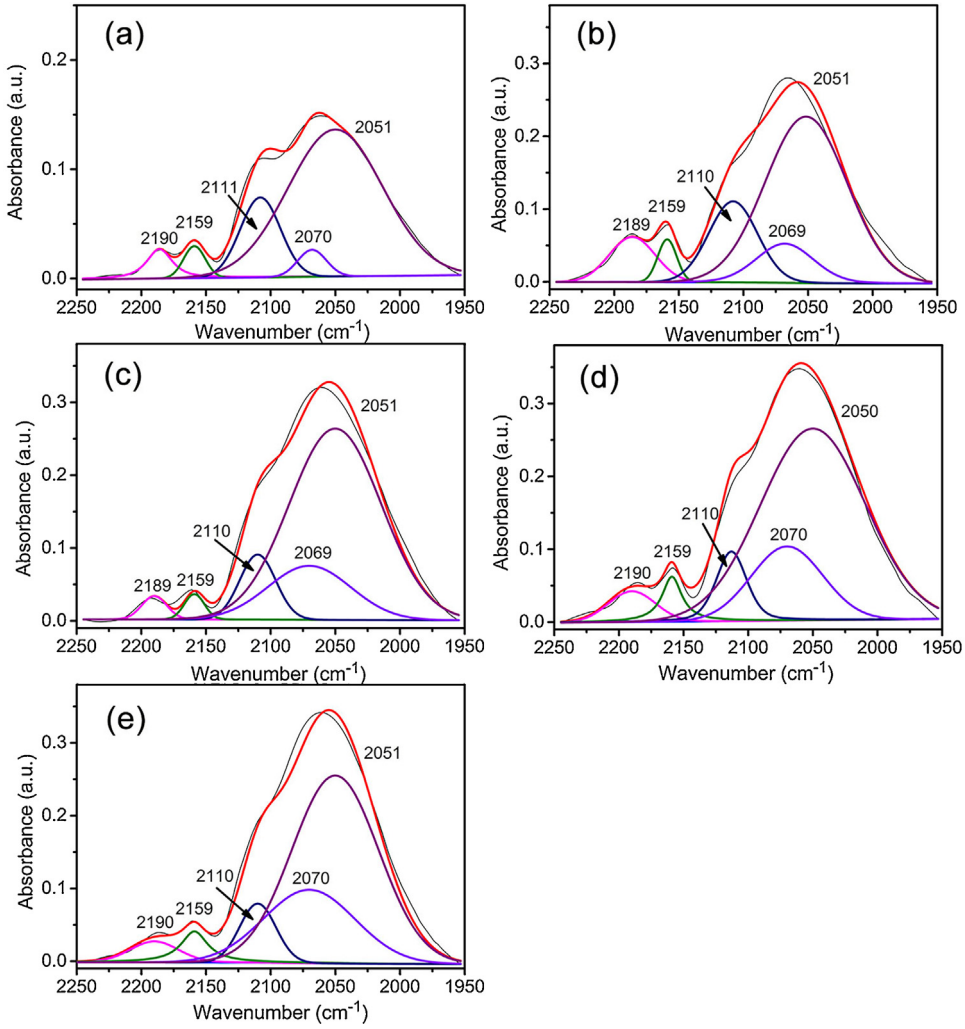

Fig. 1. in situ FT-IR spectra of CO absorbed on Catalysts 3.0CoMo (a), 3.0CoMo-1.0EDTA (b), 3.0CoMo-1.2EDTA (c), 3.0CoMo-1.4EDTA (d) and 3.0CoMo-1.6EDTA (e).

where S_F and S_P are the mass fractions of total sulfur in the feedstock and products, respectively, and O_F and O_P are the volume fractions of olefins in the feedstock and products, respectively.

The selectivity factor is defined as the ratio of the HDS activity to the olefin hydrogenation activity and is expressed as follows:

$$S = \frac{\ln(S_P/S_F)}{\ln(O_P/O_F)} \tag{18}$$

3. Results and discussion

3.1. in situ FT-IR of CO adsorption

The in situ FT-IR spectra of CO adsorbed onto the sulfided 3.0CoMo and 3.0CoMo-xEDTA catalysts are exhibited in Fig. 1. The peak at 2190 cm^{-1} is attributed to CO in interaction with Al^{3+} vacancies, the peak at 2159 cm^{-1} is due to CO connected with weakly acidic hydroxyl groups of $A1_2O_3$ by hydrogen bonds, and the peak at 2110 cm^{-1} is specific CO adsorption on active MoS_2 centers. The shoulder peaks at 2070 cm^{-1} and 2051 cm^{-1} correspond to CO interacting with the CoMoS phases [29–33]. The in situ FT-IR spectra of adsorbed CO were decomposed by the mixed Gaussian-Lorentzian function [34]. The corresponding quantitative analyses were performed based on the measured molar absorption coefficient of 33.0 cm/μmol for active CoMoS phases and the molar absorption coefficient of 16.0 cm/μmol for active MoS_2 phases [35]. The concentrations of CoMoS and MoS_2 phases for each catalyst were calculated by Formula (19), and the results are presented in Table 2. There is a linear relationship between the peak areas of CO-IR spectra and the concentrations of MoS_2 and CoMoS species (Figs. S1 and S2).

$$C = \frac{BS}{m\varepsilon} \tag{19}$$

Table 2
Concentrations of CoMoS and MoS_2 phases and HRTEM statistic results of the catalysts with different molar ratios of EDTA to Co.

Catalyst	CoMoS concentration (mmol/g)	MoS_2 concentration (mmol/g)	$\bar{L}$(nm)	$\bar{N}$	D
3.0CoMo	0.057	0.027	3.63	1.92	0.30
3.0CoMo-1.0EDTA	0.104	0.026	3.58	2.07	0.31
3.0CoMo-1.2EDTA	0.131	0.025	3.64	2.28	0.30
3.0CoMo-1.4EDTA	0.151	0.024	3.59	2.47	0.31
3.0CoMo-1.6EDTA	0.133	0.024	3.62	2.67	0.30

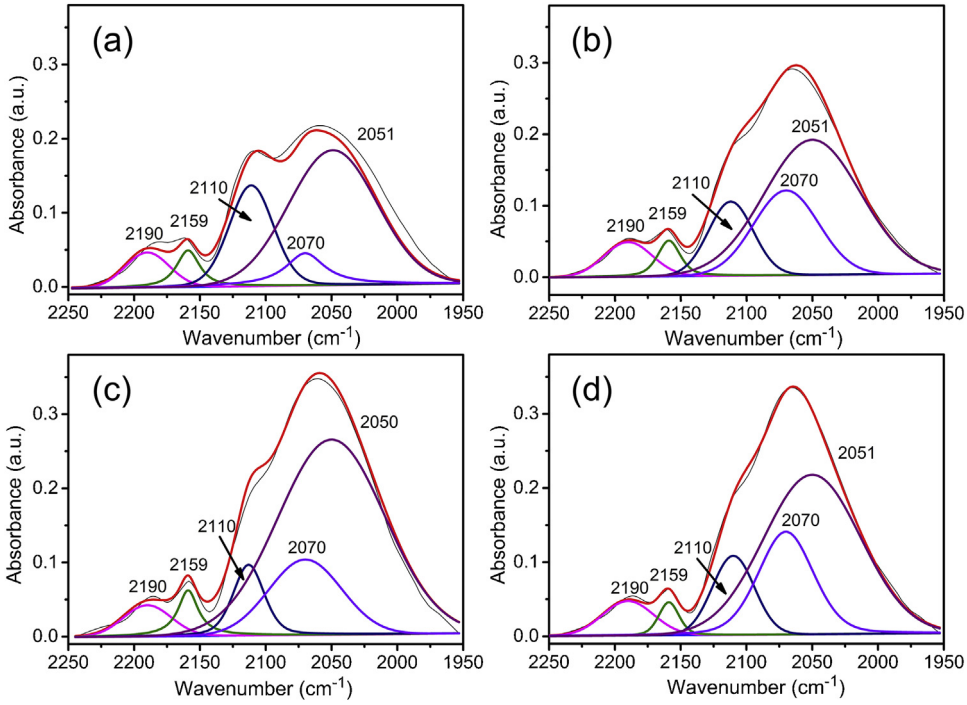

Fig. 2. in situ FT-IR spectra of CO absorbed on Catalysts 1.0CoMo-1.4EDTA (a), 2.0CoMo-1.4EDTA (b), 3.0CoMo-1.4EDTA (c) and 4.0CoMo-1.4EDTA (d).

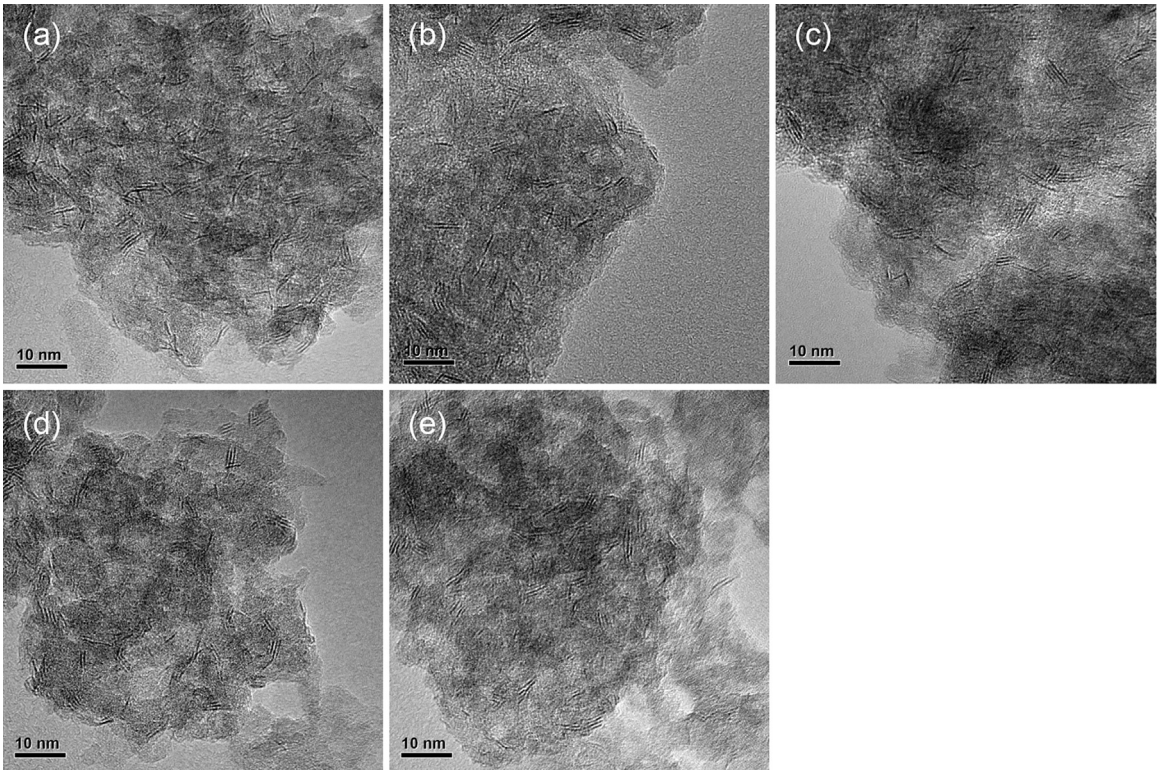

Fig. 3. HRTEM images of sulfided Catalysts 3.0CoMo (a), 3.0CoMo-1.0EDTA (b), 3.0CoMo-1.2EDTA (c), 3.0CoMo-1.4EDTA (d) and 3.0CoMo-1.6EDTA (e).

where B is the integral area of the peak; S is the cross-sectional area of the sample; m is the mass of the sample; and ε is the molar extinction coefficient.

From Table 2, the concentrations of CoMoS phases in Catalysts 3.0CoMo-xEDTA are much higher than that in Catalyst 3.0CoMo without EDTA. During the sulfurization process, the anion Co-EDTA complexes formed by the interaction between Co^{2+} cation and EDTA are structurally stable [36,37] and cannot be sulfided until molybdenum is sulfided. When the sulfurization temperature is higher than the decomposition temperature of Co-EDTA, EDTA is decomposed into gaseous species and residual carbonaceous species (Table S1); the cobalt is released from Co-EDTA and

Table 3
Concentrations of CoMoS and MoS_2 phases and HRTEM statistic results of the catalysts with different Co contents.

Catalyst	CoMoS concentration (mmol/g)	MoS_2 concentration (mmol/g)	$\bar{L}$(nm)	$\bar{N}$	D
1.0CoMo-1.4EDTA	0.079	0.050	4.02	2.05	0.28
2.0CoMo-1.4EDTA	0.113	0.037	3.76	2.22	0.30
3.0CoMo-1.4EDTA	0.151	0.024	3.59	2.47	0.31
4.0CoMo-1.4EDTA	0.128	0.029	3.20	2.55	0.34

then occupies the edge and corner sites of the already formed MoS_2 crystallites to form CoMoS phases [38]. This suggests that EDTA promotes Co coverage on the edge and corner sites of MoS_2 phases, resulting in a higher concentration of CoMoS phases in the catalysts with EDTA than in the catalyst without EDTA [21].

With an increasing EDTA content in Catalysts 3.0CoMo-xEDTA, the concentration of active CoMoS phases first increases and then decreases, reaching the maximum at Catalyst 3.0CoMo-1.4EDTA with the EDTA/Co molar ratio of 1.4. These results are explained as follows. In the preparation process of supported CoMoS catalysts, when the EDTA/Co molar ratio is less than 1.4, an increase in the EDTA content prevents the cobalt from being sulfided in advance and thereby increases the concentration of CoMoS phases. However, the EDTA/Co molar ratio higher than 1.4 causes the formation of Mo-EDTA complexes, which are only sulfided at high temperature [39]; thus, when the MoS_2 crystallites are formed, cobalt has been already converted into Co_9S_8, which cannot interact with the MoS_2 crystallites to constitute CoMoS phases [36]. As a consequence, the concentration of CoMoS phases decreases.

There is a negligible change in the concentration of active MoS_2 phases with increasing EDTA content. Type I CoMoS phases with strong metal-support interaction exist on alumina as a single-slab and monolayer structure, whereas the type II CoMoS phases with weak metal-support interaction are present as a multilayer structure [40]. Therefore, the type I phase is not fully sulfided, and the type II phase has a high degree of sulfidation [28]. As seen from the following HRTEM images, with an increasing EDTA content, the layer number of MoS_2 slabs increases, indicating that a part of the type I phases with low sulfidation has been transformed into the type II phases with high sulfidation. The reduction of MoS_2 concentration caused by Co occupation on the edge and corner sites of MoS_2 slabs is counterbalanced by the increase in MoS_2 concentration due to the enhanced sulfidation degree. As a result, the concentration of active MoS_2 phases hardly changes with increased EDTA content in the catalysts.

The in situ IR spectra of CO adsorbed on the sulfided yCoMo-1.4EDTA catalysts are presented in Fig. 2. The CO-IR spectrum of each catalyst was further decomposed by the mixed Gaussian-Lorentzian function, and the calculated concentrations of MoS_2 and CoMoS phases are presented in Table 3. With increasing cobalt content, the concentration of CoMoS phases first increases and then decreases with a maximum (0.151 mmol/g) at the cobalt content of 3.0 wt.%. However, the concentration of MoS_2 phases first decreases and then increases slightly with a minimum (0.024 mmol/g) at the cobalt content of 3.0 wt.%. These results are clarified as follows. The contents of cobalt aluminate ($CoAl_2O_4$), Co_9S_8 and CoMoS species have strong dependence on the atomic ratio of Co/Mo [41]. The increase in the cobalt content in the catalysts leads to higher cobalt coverage on the edge and corner sites of MoS_2 crystallites; thereby, the concentration of CoMoS phases increases and the concentration of MoS_2 phases decreases. When the cobalt content is higher than 3.0 wt.%, the excess addition of cobalt results in an increase of Co_9S_8 and $CoAl_2O_4$, as verified by the following XPS results; therefore, the concentration of CoMoS phases decreases and the concentration of MoS_2 phases increases.

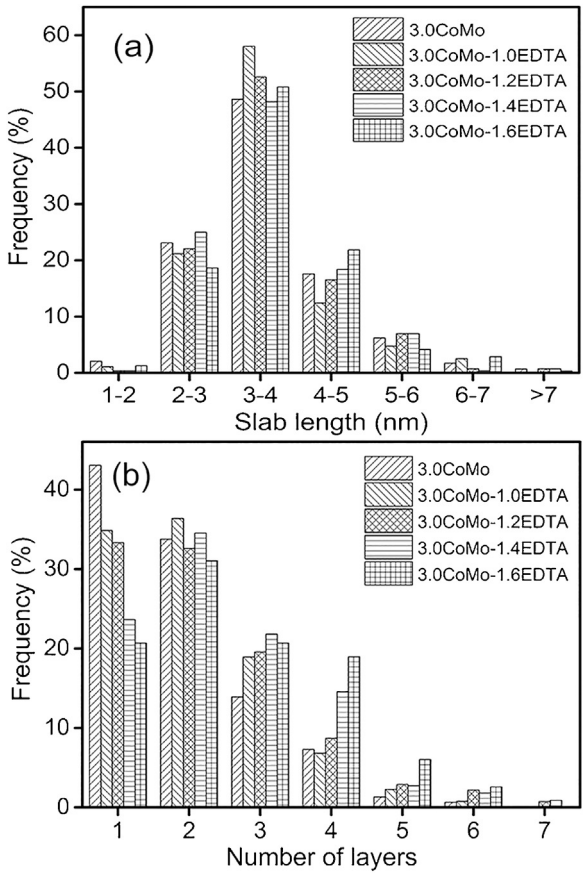

Fig. 4. Distributions of the lengths (a) and layer numbers (b) of MoS_2 slabs on sulfided Catalysts 3.0CoMo and 3.0CoMo-xEDTA.

3.2. HRTEM characterization

To obtain information regarding the morphology and distribution of MoS_2 crystallines, the sulfided catalysts were analyzed using HRTEM, and representative micrographs of Catalysts 3.0CoMo and 3.0CoMo-xEDTA are displayed in Fig. 3. The images show the edge or prism planes oriented along or roughly parallel to the electron beam direction with layer stacking spacing of 0.61-0.62 nm, matching the characteristic (002) basal planes of crystalline MoS_2 [42,43]. In the supported CoMo catalysts, the clusters of Co species are smaller than 0.5 nm, which is not in the detection range of HRTEM characterization and is not shown in HRTEM figures [44]. Therefore, the black thread-like fringes are attributed to not only MoS_2 phases but also CoMoS phases.

The statistical results of the length and stacking distributions of MoS_2 slabs on Catalysts 3.0CoMo and 3.0CoMo-xEDTA are presented in Fig. 4, and the average length and layer number of MoS_2 slabs are listed in Table 2. From Fig. 4, the length of MoS_2 slabs on each catalyst is concentrated between 3.0 and 5.0 nm; the layer number of MoS_2 slabs with the highest frequency is distributed between 2 and 4 layers. It is observed that the incorporation of EDTA in the catalysts changes the stacking distribution of MoS_2 slabs. In

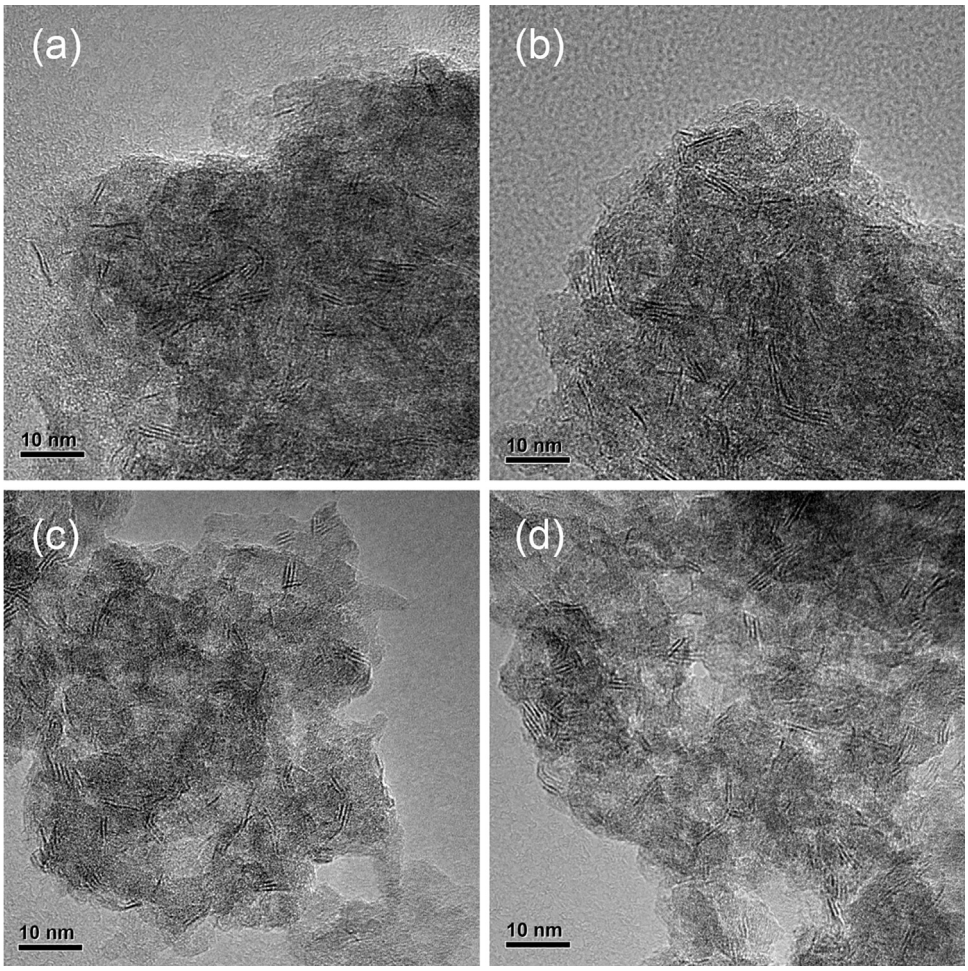

Fig. 5. HRTEM images of Catalysts 1.0CoMo-1.4EDTA (a), 2.0CoMo-1.4EDTA (b), 3.0CoMo-1.4EDTA (c) and 4.0CoMo-1.4EDTA (d).

catalyst 3.0CoMo without EDTA, mostly MoS_2 slabs of 1 ~ 2 layers are observed, and multi-stacked MoS_2 slabs with more than 3 layers are few. With an increased EDTA content in catalyst 3.0CoMo-xEDTA, the percentage of MoS_2 slabs with 1 layer decreases and those with 2 layers has minor change, whereas the percentage of MoS_2 slabs with 3 ~ 4 layers increases. From Table 2, the average length and stacking layer number of MoS_2 slabs on Catalyst 3.0CoMo are 3.63 nm and 1.92 layers, and the dispersion degree of active MoS_2 slabs on Catalyst 3.0CoMo is 0.30. The addition of EDTA to Catalyst 3.0CoMo results in an increase in the average stacking layer number of MoS_2 slabs with an increased EDTA content. The increase in the EDTA content does not significantly alter the average length or dispersion of MoS_2 slabs.

Typical HRTEM images of the sulfided yCoMo-1.4EDTA catalysts are presented in Fig. 5. The statistical results of the stacking and length distributions of MoS_2 slabs on these catalysts are shown in Fig. 6. The average length and stacking number of MoS_2 slabs on these catalysts are presented in Table 3. From Fig. 6, the length of MoS_2 slabs on each catalyst is predominantly distributed between 3.0 and 5.0 nm, and the stacking layer number of MoS_2 slabs is between 2 and 4 layers. The stacking distribution of MoS_2 slabs is also adjusted with the increasing Co content. With the increased Co content in Catalysts yCoMo-1.4EDTA, the percentage of MoS_2 slabs with 1 ~ 2 layers decreases (from 75.2% of 1.0CoMo-1.4EDTA to 49.1% of 4.0CoMo-1.4EDTA), and there is an increase in the percentage of MoS_2 slabs with 3 ~ 4 layers (from 22.3% of 1.0CoMo-1.4EDTA to 40.0% of 4.0CoMo-1.4EDTA). From Table 3, increasing Co content leads to a decrease in the average slab length (from 4.02 nm of Catalyst 1.0CoMo-1.4EDTA to 3.20 nm of Catalyst 4.0CoMo-1.4EDTA) and to an increase in the average stacking number of MoS_2 slabs (from 2.05 of Catalyst 1.0CoMo-1.4EDTA to 2.55 of Catalyst 4.0CoMo-1.4EDTA). In addition, the dispersion of MoS_2 slabs increases gradually from 0.28 of Catalyst 1.0CoMo-1.4EDTA to 0.34 of Catalyst 4.0CoMo-1.4EDTA with increasing Co content in these catalysts. These results are explained as follows. With an increasing Co content in these catalysts, Co would be continuously captured by MoS_2 slabs and decorated on the edge and corner sites of MoS_2 slabs, which can stabilize the multilayered stacks of MoS_2 slabs acting as a binder between two neighboring layers [45,46]. Co promotes the stacking of MoS_2 slabs and inhibits the growth of MoS_2 slabs along the basal direction; therefore, the average length of MoS_2 slabs decreases, and the dispersion of MoS_2 slabs increases [47].

3.3. XPS characterization

The surface components and chemical states of metal species on the sulfided catalysts were studied by XPS survey spectra. Binding energies in the ranges of 775–805 eV and 224–238 eV are ascribed to Co2p and Mo3d spectra [48]. In the high-resolution scans and corresponding fitting curves of the Co2p XPS spectra (Figs. 7 and 8 and the peaks at 778.8 and 793.9 eV in the Co2p deconvolution spectra are attributed to the $Co2p_{3/2}$ and $Co2p_{1/2}$ levels of CoMoS phases; the binding energies at 778.2 and 793.2 eV are ascribed to the $Co2p_{3/2}$ and $Co2p_{1/2}$ levels of Co_9S_8 species; and those at 781.5 and 797.5 eV are ascribed to Co^{2+} species ($CoAl_2O_4$) (Table S3) [41].

Table 4
Fitting results of XPS on the sulfided yCoMo-1.4EDTA catalysts.

Catalyst	Co fraction (%)			Mo fraction (%)			$r(MoS_2)_c$	$r(CoMoS)_e$	$r(CoMoS)_e/r(MoS_2)_c$
	CoMoS	Co_9S_8	Co^{2+}	MoS_2	Mo^{5+}	Mo^{6+}			
3.0CoMo	22.7	19.7	57.6	49.7	20.7	29.7	0.265	0.661	2.49
3.0CoMo-1.0EDTA	34.0	17.8	48.2	52.9	19.6	27.5	0.192	0.798	4.15
3.0CoMo-1.2EDTA	38.3	17.6	44.1	58.4	19.4	22.2	0.156	0.839	5.38
3.0CoMo-1.4EDTA	44.1	13.4	42.6	60.3	19.8	19.8	0.145	0.865	5.96
3.0CoMo-1.6EDTA	40.7	15.8	43.5	62.8	19.5	17.7	0.150	0.846	5.64
1.0CoMo-1.4EDTA	36.2	22.3	41.5	57.9	18.6	23.5	0.305	0.589	1.93
2.0CoMo-1.4EDTA	40.7	16.4	42.9	59.8	19.1	21.0	0.228	0.749	3.28
4.0CoMo-1.4EDTA	34.2	24.3	41.5	60.6	20.3	19.1	0.192	0.817	4.26

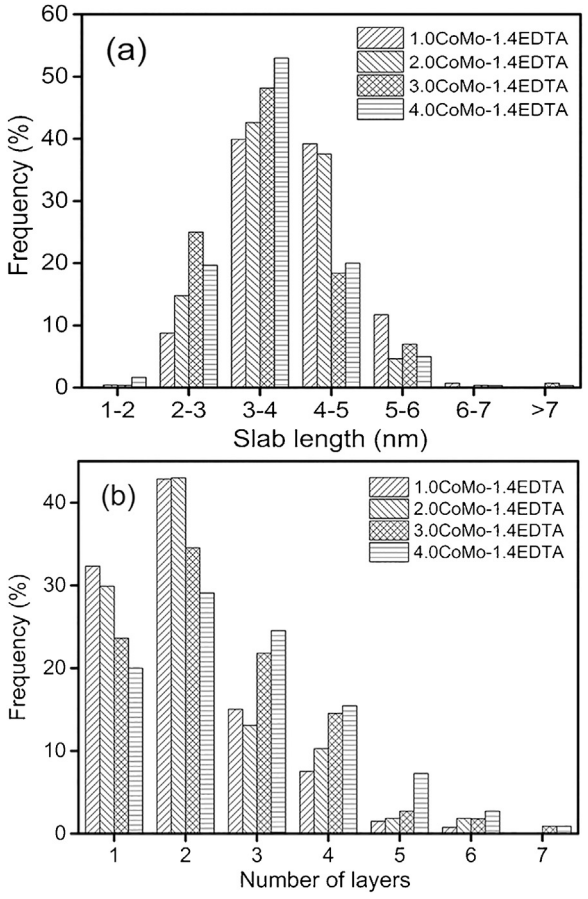

Fig. 6. Distributions of the lengths (a) and layer numbers (b) of MoS_2 slabs on the sulfided yCoMo-1.4EDTA catalysts.

The Co2p spectra were decomposed according to the literature [49]; the relative concentrations of different Co species on the sulfided catalysts are listed in Table 4. The reference 3.0CoMo catalyst has the lowest percentage of cobalt in the CoMoS species (22.7%) and the highest percentage of Co^{2+} species on the surface, and incorporating EDTA in the 3.0CoMo catalyst increases the percentage of CoMoS species. With an increasing EDTA content in Catalysts 3.0CoMo-xEDTA, the relative content of CoMoS species first increases and then decreases, reaching a maximum at Catalyst 3.0CoMo-1.4EDTA with the EDTA/Co molar ratio of 1.4; the relative content of Co_9S_8 species first decreases and then increases with a minimum at the EDTA/Co molar ratio of 1.4, whereas the relative content of Co^{2+} species decreases gradually. The relative percentage content of cobalt species is influenced by the atomic ratio of Co/Mo. With increasing Co/Mo atomic ratio, the relative content of CoMoS species first increases and then decreases with a maximum at the cobalt content of 3.0 wt.%; the relative content of Co_9S_8 species first decreases and then increases with a minimum at the cobalt content of 3.0 wt.%, whereas the relative content of Co^{2+} species has no obvious change.

The measured spectra and fitted XPS patterns of Mo3d for the sulfided catalysts are presented in Figs. 9 and 10. For the $Mo3d_{5/2}$ energy level, three peaks are observed at 229.0, 229.6 and 232.8 eV, which are attributed to MoS_2 species (Mo^{4+}), oxysulfide MoO_xS_y compounds (Mo^{5+}) and MoO_3 species (Mo^{6+}), respectively [50]. For the $Mo3d_{3/2}$ energy level, the binding energies at 232.0, 232.9 and 236.0 eV are ascribed to the MoS_2 species (Mo^{4+}), oxysulfide MoO_xS_y compounds (Mo^{5+}) and MoO_3 species (Mo^{6+}), respectively [50]. The spectra also include the S2s peak at 226.0 eV (Table S3).

The Mo3d spectra were decomposed, and the relative contents of MoS_2, MoO_xS_y and MoO_3 species are listed in Table 4. Catalyst 3.0CoMo without EDTA has the lowest percentage of molybdenum in MoS_2 species (49.7%) and the highest percentage of MoO_3 species on the surface. With the increasing EDTA content in Catalysts 3.0CoMo-xEDTA, the relative content of MoS_2 species increases, whereas the relative contents of MoO_xS_y and MoO_3 species decrease gradually. The addition of Co has minor influence on the sulfidation of molybdenum [49]; the relative contents of MoS_2 species, MoO_xS_y compounds and MoO_3 species do not significantly change.

Using Eq. (14) to calculate the ratio between the amount of MoS_2 atoms on the corner and the amount of CoMoS and MoS_2 atoms on the corner ($r(MoS_2)_c$) requires the concentrations of CoMoS and MoS_2 phases at the corner sites, and using Eq. (15) to calculate the ratio between the amount of CoMoS atoms on the edge and the amount of CoMoS and MoS_2 atoms on the edge ($r(CoMoS)_e$) requires the concentrations of CoMoS and MoS_2 phases at the edge sites. The concentrations of active CoMoS phases and MoS_2 phases are measured by CO-IR characterization, and then the concentrations of CoMoS phases and MoS_2 phases at the edge and corner sites are calculated as follows. The active MoS_2 phases only located at the accessible edge and corner positions, and the rest MoS_2 species do not have reactivity even though they could be detected by XPS [50,51]. Thus, it is necessary to use HRTEM characterization to figure out the edge/corner ratio and calculate the concentrations of active MoS_2 phases at the accessible edge and corner positions. The Co species are too small to be detected by HRTEM characterization; therefore, taking into account the edge-to-corner ratio of a MoS_2 slab calculated by HRTEM characterization and the promoter ratio in the slab of CoMoS phase calculated by XPS characterization, the edge/corner ratio of CoMoS phases are determined. Thus, the concentrations of active CoMoS phases at the edge and corner sites are obtained. Consequently, $r(MoS_2)_c$ and $r(CoMoS)_e$ are calculated by using Eq. (14) and Eq. (15), respectively.

Based on the CO-IR, XPS and HRTEM characterizations, the ratio $r(CoMoS)_e$ and the ratio $r(MoS_2)_c$ were calculated, and the results are presented in Table 4. With an increasing EDTA content, the $r(CoMoS)_e$ value first increases and then decreases, reaching the maximum when the EDTA/Co molar ratio is 1.4, and the $r(MoS_2)_c$ value first decreases and then increases, reaching the minimum

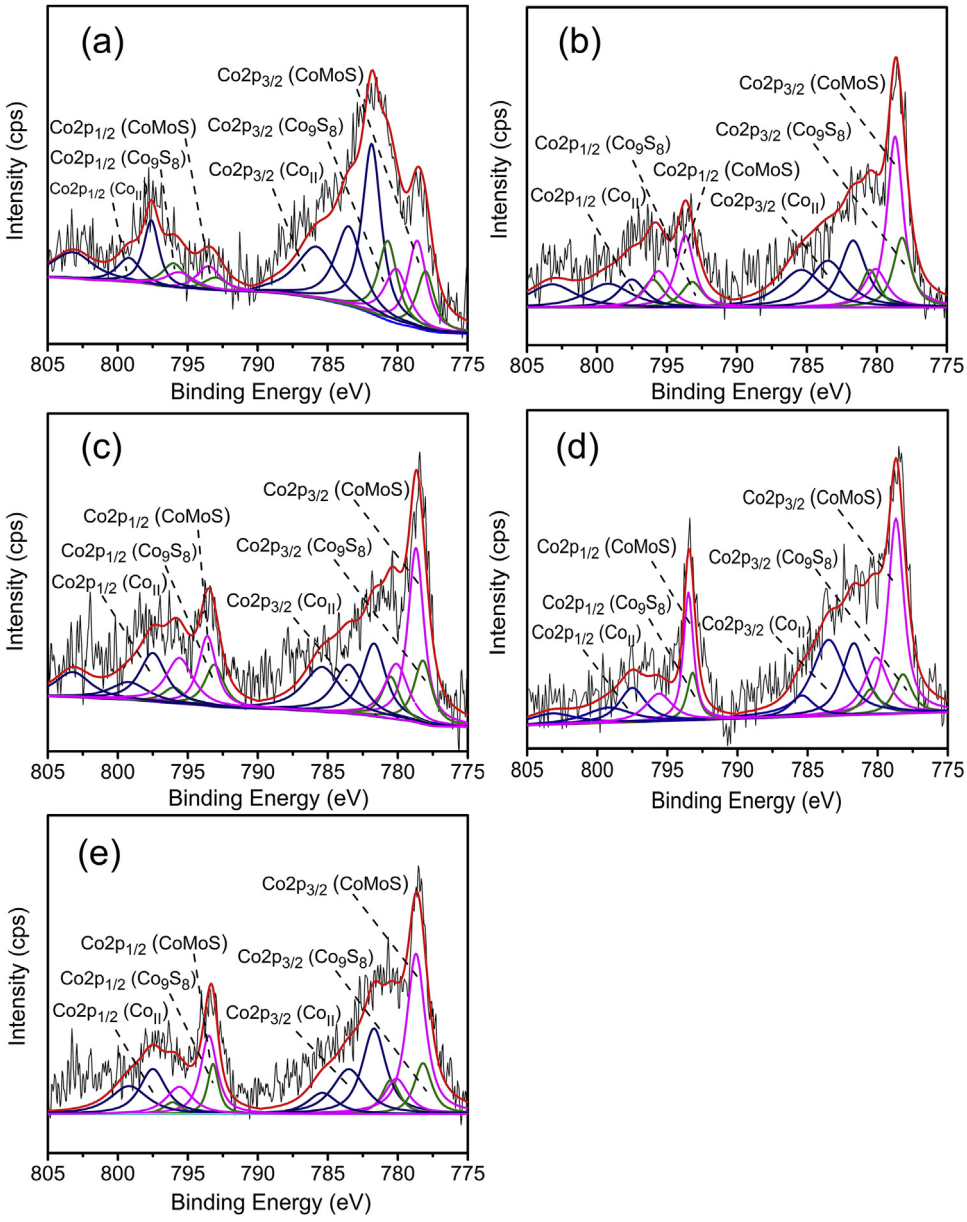

Fig. 7. Co2p XPS spectra of Catalysts 3.0CoMo (a), 3.0CoMo-1.0EDTA (b), 3.0CoMo-1.2EDTA (c), 3.0CoMo-1.4EDTA (d) and 3.0CoMo-1.6EDTA (e).

when the EDTA/Co molar ratio is 1.4. With an increasing Co content, the $r(\mathrm{CoMoS})_e$ value first increases and then decreases with a maximum at the cobalt content of 3.0 wt.%, and the $r(\mathrm{MoS_2})_c$ value first decreases and then increases with a minimum at the cobalt content of 3.0 wt.%.

3.4. Catalytic activity

The activity assessment results show that Catalyst 3.0CoMo without EDTA exhibits poor selective HDS performance, with a HDS ratio of 71.0%, the OHYD degree of 11.8%, and the selectivity factor of 9.9. The HDS activity, OHYD activity and selectivity factor of the $\mathrm{CoMo/Al_2O_3}$ catalysts with EDTA were correlated with the molar ratio of EDTA/Co; the results are displayed in Figs. 11 and 12. Compared with Catalyst 3.0CoMo, the addition of EDTA improves the HDS activity and selectivity and has a minor influence on the OHYD activity. With an increasing EDTA/Co molar ratio, the HDS activity and the selectivity factor first increase and then decrease, with the maximal HDS ratio (92.9%) and the optimal selectivity factor (24.6) at the EDTA/Co molar ratio of 1.4. The increase of EDTA/Co molar ratio has a minor influence on the OHYD activity. The modification of Co on Mo sites (edge and corner sites) produces the CoMoS phases, which significantly promote the HDS reaction, but play a minor role in the OHYD reaction [52,53]. By comparing the results of Table 2 and Fig. 11, the concentration of CoMoS phases first increases and then decreases with the increasing EDTA content, in accordance with the variation trend of HDS activity; the OHYD reactivity has no obvious change with the increasing EDTA content.

The HDS activity, OHYD activity and selectivity factor of the EDTA-containing catalysts with different Co loadings are presented in Figs. 13 and 14. With the increasing Co content, the HDS activity and the selectivity factor first increase and then decrease with the optimal values at the CoO loading of 3.0 wt.%, whereas the olefin saturation first decreases and then increases with the minimal OHYD activity at the CoO loading of 3.0 wt.%. The addition of cobalt to the MoS_2 catalysts is beneficial for improving HDS activity and selectivity [54,55]. Increasing the Co content in the MoS_2 catalysts

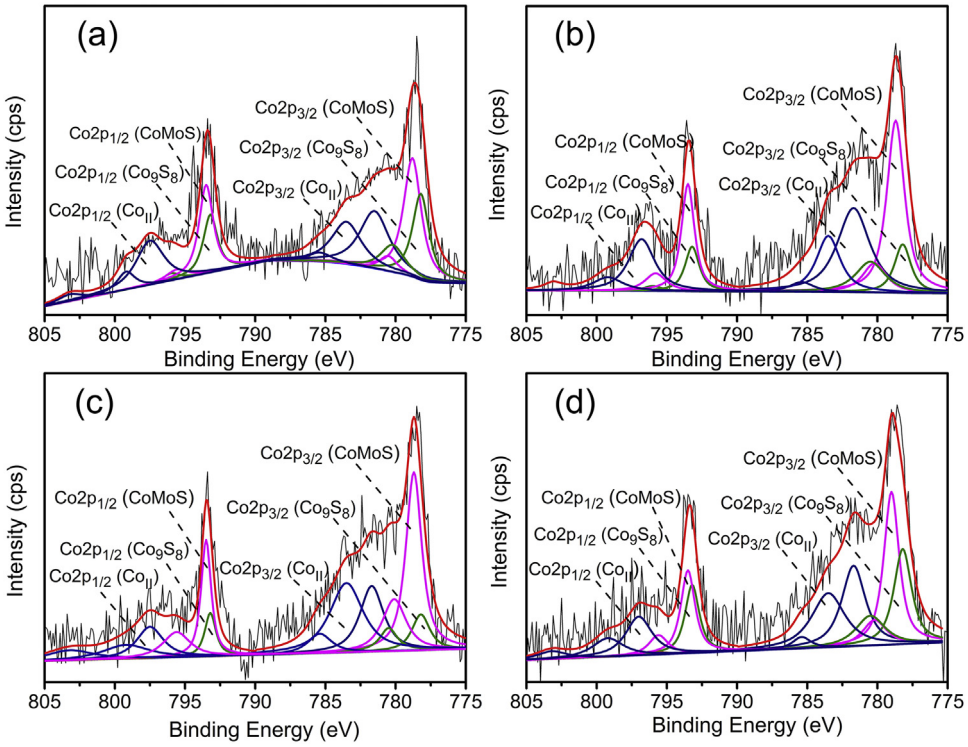

Fig. 8. Co2p XPS spectra of Catalysts 1.0CoMo-1.4EDTA (a), 2.0CoMo-1.4EDTA (b), 3.0CoMo-1.4EDTA (c) and 4.0CoMo-1.4EDTA (d).

promotes the formation of CoMoS active phases, which enhances the HDS activity; the incorporation of Co ions into the edges of MoS_2 crystallites reduces the number of coordinately unsaturated Mo sites on the edges of MoS_2 crystallites and thereby suppresses olefin hydrogenation. The higher modification degree of MoS_2 crystallites by Co improves the HDS activity and selectivity [52]. When the cobalt content is higher than 3.0 wt.%, the excess addition of cobalt results in the increase of Co_9S_8 and $CoAl_2O_4$, the decreased concentration of CoMoS phases and the slightly increased concentration of MoS_2 phases (Table 3); therefore, the HDS activity and selectivity decrease, while the OHYD activity increases.

From Figs. 11–14, we conclude that the catalyst with the CoO loading of 3.0 wt.% and the EDTA/Co molar ratio of 1.4 has the best HDS activity and selectivity of the two series of catalysts, giving a HDS ratio of 92.9%, an OHYD degree of 10.2%, and a selectivity factor of 24.6. The typical catalysts (3.0CoMo, 3.0CoMo-1.4EDTA and 4.0CoMo-1.4EDTA) have constant HDS and OHYD activities during 96 h test, demonstrating their good activity stability (Fig. S3). The relative contents of CoO, MoO_3 and Al_2O_3 in the used catalysts are almost the same as those of the fresh catalysts listed in Table 1, which indicates that the cobalt and molybdenum species are stable on the Al_2O_3 support (Table S2).

3.5. Influences of the concentration and the microstructure of CoMoS and MoS_2 active phases on the HDS/OHYD reaction

3.5.1. HDS and OHYD activities versus the concentration of CoMoS and MoS_2 active phases

To illustrate the influence of CoMoS concentration on the thiophene HDS reaction, the concentrations of CoMoS active phases with the different catalysts (Tables 2 and 3) were correlated with the HDS activities (Figs. 11–13), and the results are shown in Fig. 15. There is a direct proportional relationship between the concentration of CoMoS phases and the HDS activity, thus indicating the promotional effect of CoMoS phases on the HDS reaction. In the CoMoS phases, the promoter Co donates electrons to Mo, and an increase in number of electrons on Mo would result in stronger binding to the heterocyclic ring sulfur and further weaken the C-S bonds in the ring through back-donation into the ring π^* orbital [56], which enhance the breaking of C-S bonds in thiophene and thereby improve the HDS activity of the catalysts.

To investigate the effect of CoMoS concentration on the OHYD reaction, the concentrations of CoMoS phases accompanied with approximately the same concentration of MoS_2 phases (Table 2) were correlated with the OHYD activity (Fig. 11), and the results are shown in Fig. 16. In the precondition of the constant concentration of MoS_2 phases, the change in the concentration of CoMoS phases has a negligible effect on the OHYD activity. This phenomenon is explained as follows. The interaction between CoMoS active phases and olefin through the C=C double bond with π electrons is much weaker than that between CoMoS phases and thiophene [57]; therefore, the change in the concentration of CoMoS phases has a much lower influence on the OHYD activity than on the HDS activity.

In view of the negligible influence of CoMoS concentration on the OHYD activity, the MoS_2 concentrations in the catalysts were adjusted by changing the Co content; the correlation of the OHYD activity with the MoS_2 concentrations is illustrated in Fig. 17. With decreasing MoS_2 concentration, the OHYD activity obviously decreases, indicating that the olefin saturation is closely related to the number of MoS_2 phases in the catalysts. This result demonstrates that the reaction of olefin saturation occurs on the MoS_2 active phases.

3.5.2. HDS and OHYD activities versus the microstructure of CoMoS and MoS_2 active phases with varying MoS_2 concentrations

The morphology of CoMoS phases is an important factor influencing the HDS/OHYD selectivity of transition metal sulfide (TMS) catalysts [20,27]. In the literature [19], the edge sites/corner sites ratio of supported MoS_2 slabs $(f_e/f_c)_{Mo}$ was selected as the parameter to assess the selectivity factor of the un-promoted or Co-promoted MoS_2 catalysts. Li et al. proposed that the

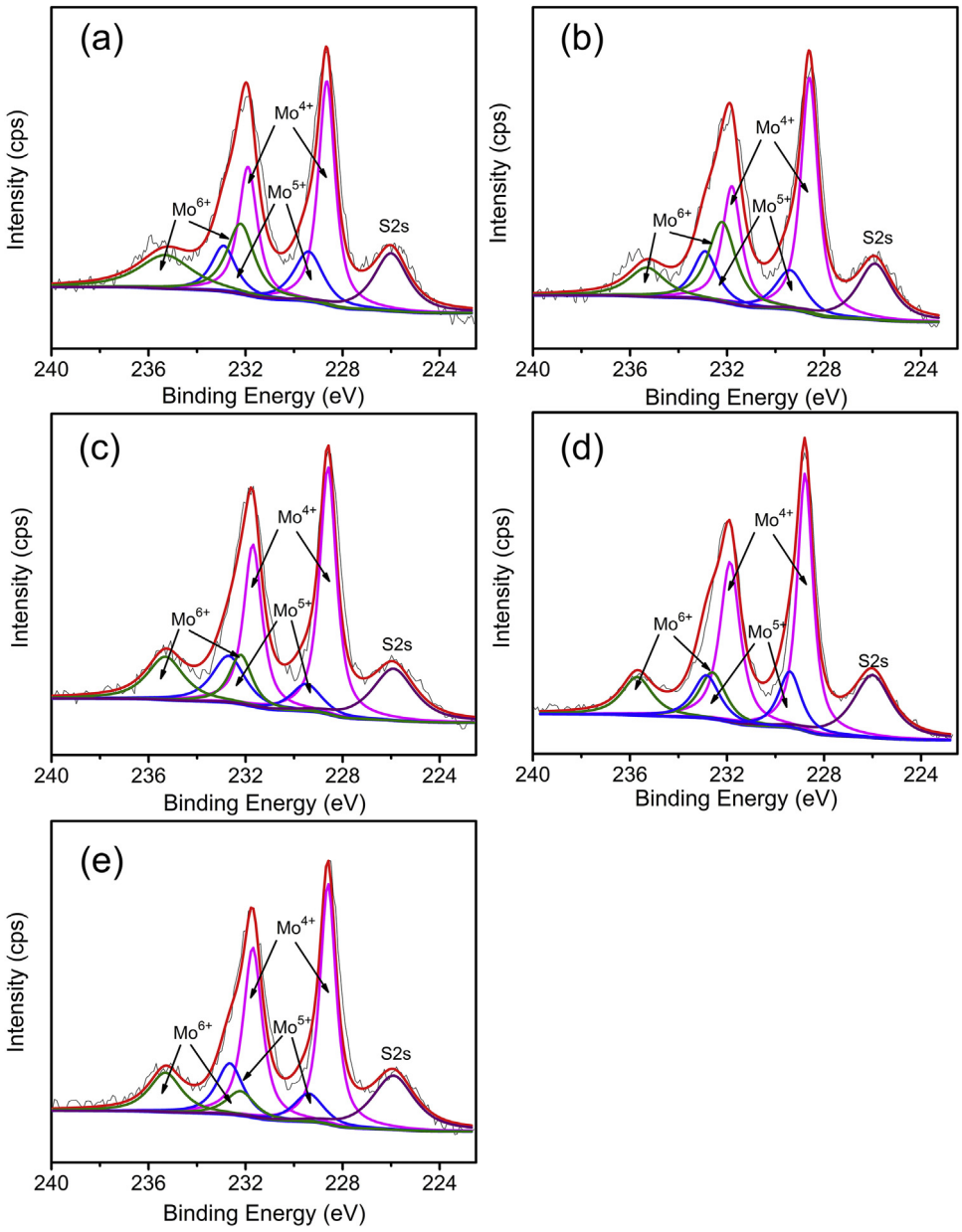

Fig. 9. Mo3d XPS spectra of Catalysts 3.0CoMo (a), 3.0CoMo-1.0EDTA (b), 3.0CoMo-1.2EDTA (c), 3.0CoMo-1.4EDTA (d) and 3.0CoMo-1.6EDTA (e).

HDS/OHYD selectivity correlated linearly with the slab length and the edge/corner ratio of MoS_2 phases [19]. According to Formula (3), the slab length ($\bar{L}$) is directly proportional to the edge sites/corner sites ratio; therefore, the parameters ($\bar{L}$ and $(f_e/f_c)_{Mo}$) have a linear relationship with the HDS/OHYD selectivity factor [19]. However, $\bar{L}$ or $(f_e/f_c)_{Mo}$ does not account for the concentration of CoMoS phases and the distribution of Co atoms at the edge and corner sites on MoS_2 slabs. Nikulshin et al. reported that the HDS/OHYD selectivity factor depends linearly on the ratio of the amount of edge Co atoms to the amount of corner Co atoms $\left(\left(f_e/f_c\right)_{CoMo}\right)$ [20], but this parameter only represents the edge-to-corner ratio of the CoMoS active phases and does not consider the relationship between the MoS_2 active phases and HDS/OHYD selectivity.

The CoMoS and MoS_2 active phases coexist in the sulfided CoMo catalysts [58]; therefore, it is necessary to correlate the microstructures of both CoMoS and MoS_2 active phases with the HDS and OHYD activities. For this purpose, the $r(\mathrm{CoMoS})_e/r(\mathrm{MoS_2})_c$ ratio was introduced, which represents the ratio between the proportion of CoMoS in the edge's CoMoS and MoS_2 active phases and the proportion of MoS_2 in the corner's CoMoS and MoS_2 active phases (Table 4). Catalysts 3.0CoMo-xEDTA have higher $r(\mathrm{CoMoS})_e/r(\mathrm{MoS_2})_c$ ratios than Catalyst 3.0CoMo. With an increasing EDTA content in Catalysts 3.0CoMo-xEDTA, the $r(\mathrm{CoMoS})_e/r(\mathrm{MoS_2})_c$ ratio first increases and then decreases with the maximal ratio (5.96) at the EDTA/Co molar ratio of 1.4. These results are explained as follows. The increase in the EDTA content has minor influence on the MoS_2 concentration and the average length of MoS_2 slabs (Table 2), and thereby the concentrations of MoS_2 phases at the edge and corner sites have no obvious change. With an increasing EDTA content, the concentration of active CoMoS phases first increases and then decreases, reaching the maximum when the EDTA/Co molar ratio is 1.4. As a consequence, the concentration of CoMoS phases at the edge sites reaches the maximum at the EDTA/Co molar ratio of 1.4, resulting in the maximal $r(\mathrm{CoMoS})_e/r(\mathrm{MoS_2})_c$ ratio.

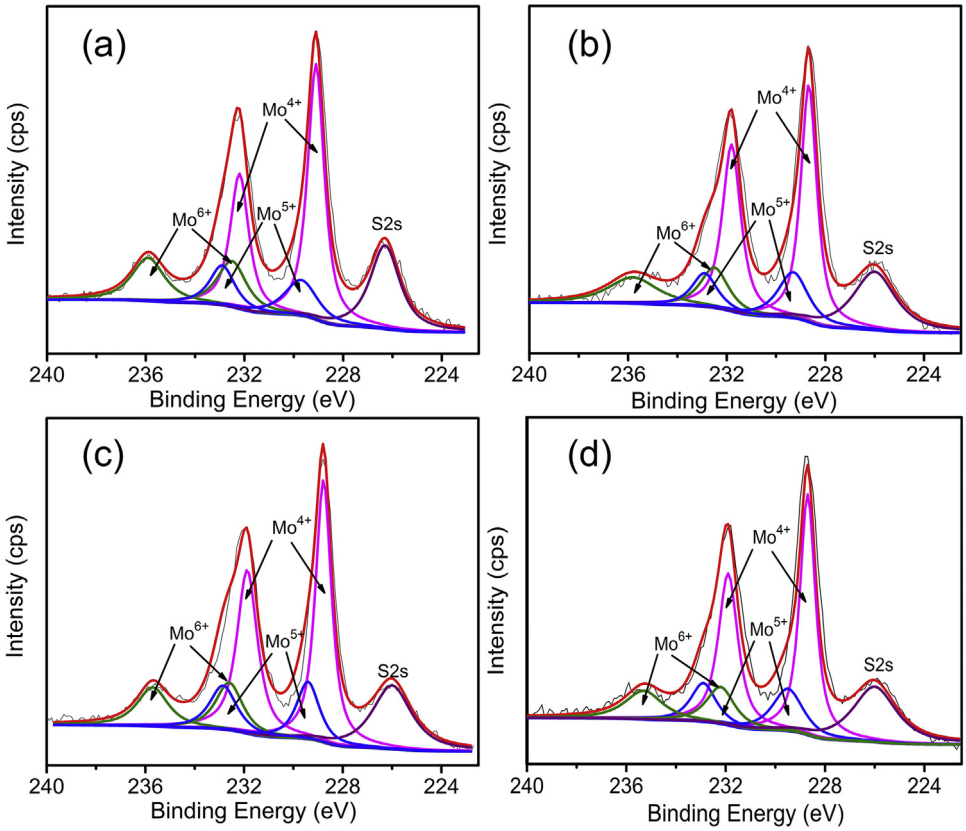

Fig. 10. Mo3d XPS spectra of Catalysts 1.0CoMo-1.4EDTA (a), 2.0CoMo-1.4EDTA (b), 3.0CoMo-1.4EDTA (c) and 4.0CoMo-1.4EDTA (d).

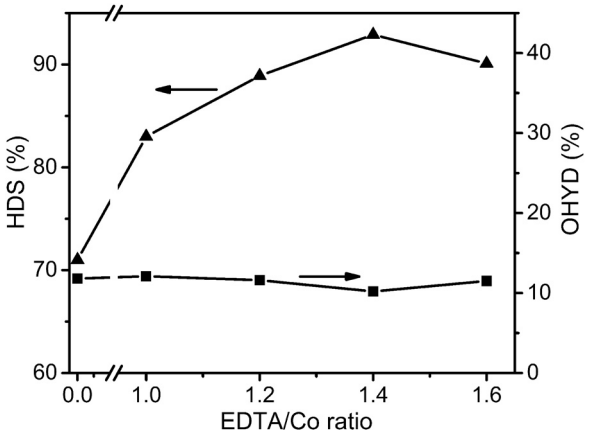

Fig. 11. HDS and OHYD activities of the catalysts with different atomic ratios of EDTA to Co.

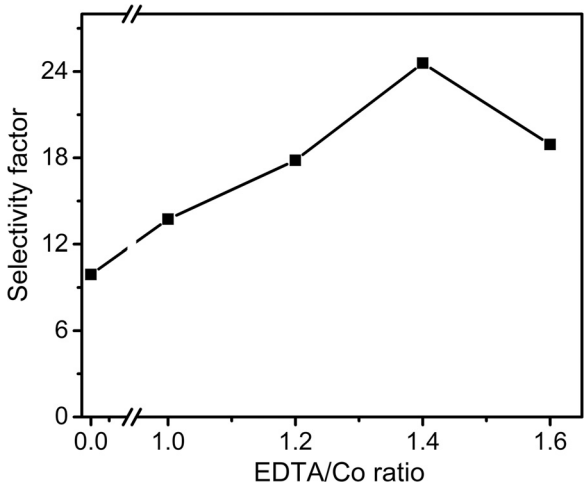

Fig. 12. Effect of EDTA/Co atomic ratio on the selectivity factor of Catalysts 3.0CoMo and 3.0CoMo-xEDTA.

With an increasing cobalt content, the $r(CoMoS)_e/r(MoS_2)_c$ ratio first increases and then decreases with a maximum at the cobalt content of 3.0 wt.%. The increase in the cobalt content in the catalysts leads to higher cobalt coverage on the edge and corner sites of MoS_2 crystallites; therefore, the concentrations of CoMoS phases at the edge sites reach the maximum and the concentrations of MoS_2 phases at the corner sites reach the minimum at the cobalt content of 3.0 wt.%. As a result, the ratio $r(CoMoS)_e/r(MoS_2)_c$ reaches the maximum at the cobalt content of 3.0 wt.%.

The relationship between the HDS and OHYD activities with this ratio is illustrated in Fig. 18. The HDS activity increases with the increase of the $r(CoMoS)_e/r(MoS_2)_c$ ratio, whereas the OHYD activity decreases with the increase of the $r(CoMoS)_e/r(MoS_2)_c$ ratio, suggesting that the HDS reaction occurs primarily at the edge of CoMoS active phases, whereas the OHYD reaction occurs mainly at the corner of MoS_2 active phases. The Mo in the edge's CoMoS active phases has a higher *d* electron density than the Mo in MoS_2 active phases at edge sites, which would strengthen the interaction between Mo and the ring sulfur atom in thiophene [56]. Therefore, the HDS reaction occurs primarily at the edge of CoMoS active phases. The corner sites of MoS_2 phases easily adsorb H_2 molecules and promote the dissociation of molecular H_2 because of their higher degree of coordinative unsaturation than that of the edge's MoS_2 sites [17]; moreover, the weak interaction between CoMoS active phases and olefin through the C=C double bond would depress the hydrogenation reaction [57]. As a consequence,

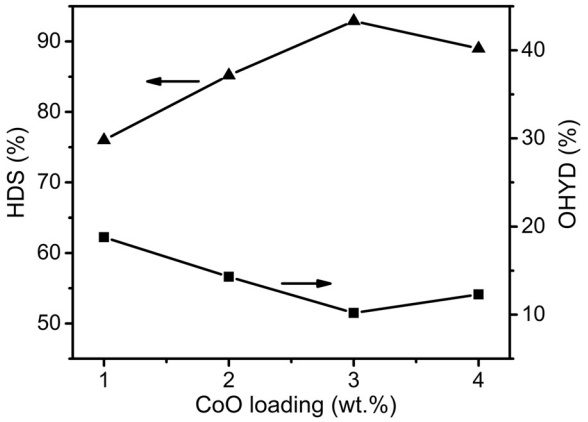

Fig. 13. HDS and OHYD activities of the catalysts with different Co contents.

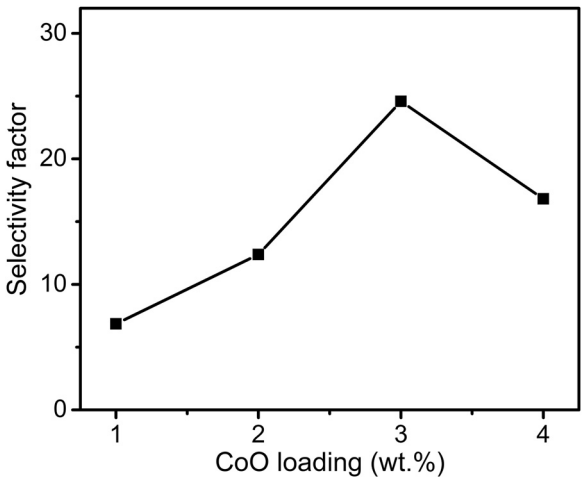

Fig. 14. Effect of Co content on the selectivity factor of Catalysts yCoMo-1.4EDTA.

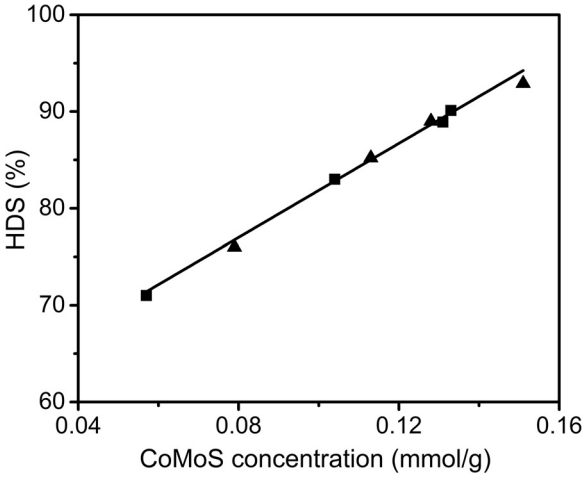

Fig. 15. Correlation of the HDS activity with the CoMoS concentration (solid squares: CoMoS concentrations of 3.0CoMo and 3.0CoMo-xEDTA catalysts, solid triangles: CoMoS concentrations of yCoMo-1.4EDTA catalysts).

the OHYD reaction occurs mainly at the corner of MoS_2 active phases.

According to the above analyses, the catalyst with low $r(CoMoS)_e$ ratio and high $r(MoS_2)_c$ ratio has less CoMoS active phases at the edge sites and more MoS_2 active phases at the corner sites, resulting in its lower activity and selectivity for thiophene

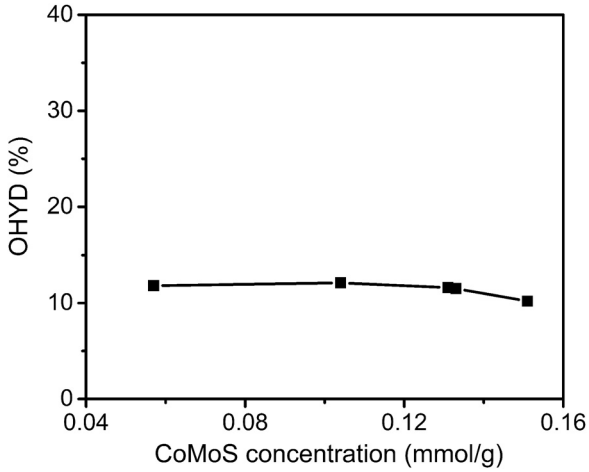

Fig. 16. Correlation of the OHYD activity with the CoMoS concentration in the precondition of the constant concentration of MoS_2 phases.

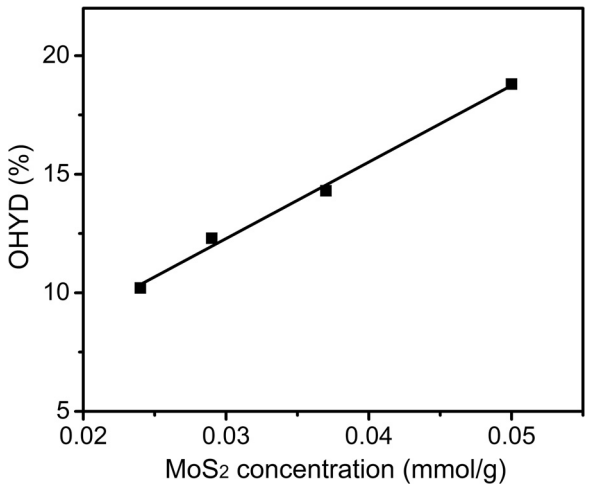

Fig. 17. Correlation of the OHYD activity with the MoS_2 concentration.

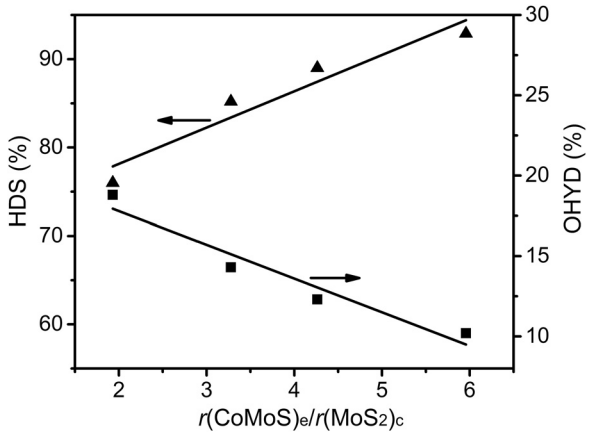

Fig. 18. Relationship between the HDS selectivity factor and the $r(CoMoS)_e/r(MoS_2)_c$ ratio over Catalysts yCoMo-1.4EDTA.

HDS; the catalyst with high $r(CoMoS)_e$ ratio and low $r(MoS_2)_c$ ratio has more CoMoS active phases at the edge sites and less MoS_2 active phases at the corner sites, greatly improving its activity and selectivity for thiophene HDS (Fig. 19).

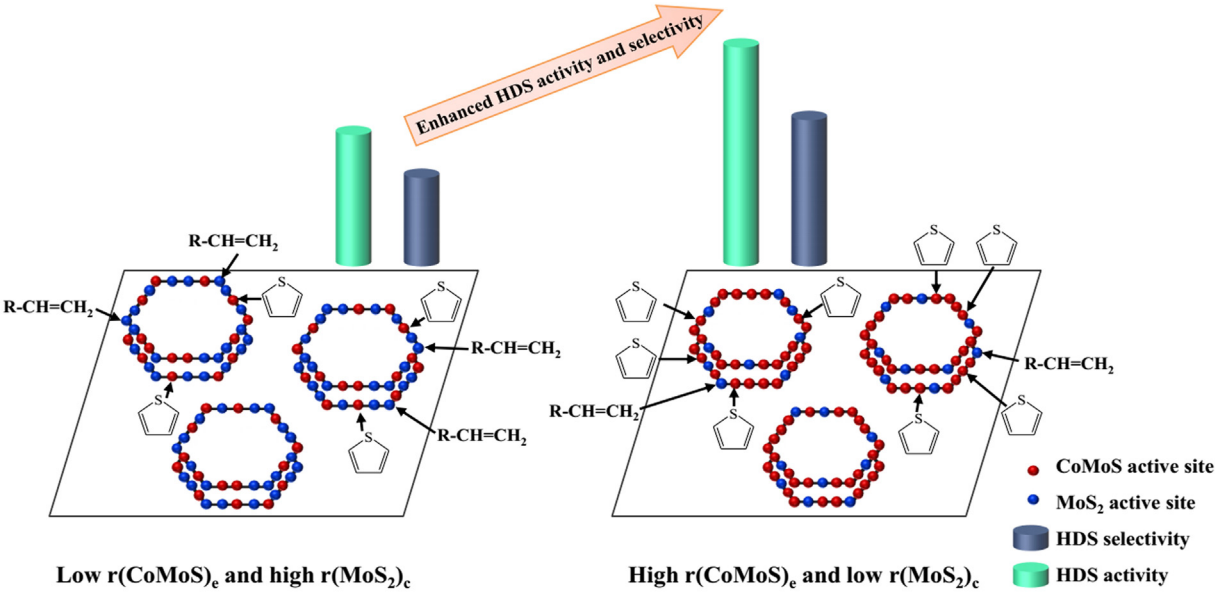

Fig. 19. Correlation between the HDS activity/selectivity and the microstructure of CoMoS and MoS_2 active phases.

4. Conclusions

A series of $CoMo/Al_2O_3$ catalysts with different ethylenediaminetetraacetic acid (EDTA)/Co molar ratios and another series of EDTA-containing $CoMo/Al_2O_3$ catalysts with different cobalt contents were prepared, and the properties of the active metal phases of these catalysts were systematically correlated with the HDS selectivity of these catalysts. The results show that in the precondition of approximately the same concentration of MoS_2 phases, an increase in the concentration of CoMoS phases had a negligible influence on the reactivity of olefin hydrogenation but had a promoting effect on HDS reactivity, indicating the insensitivity of CoMoS phases to the reaction of olefin hydrogenation. In contrast, an increase in the concentration of MoS_2 phases markedly enhanced the olefin hydrogenation activity of the $CoMo/Al_2O_3$ catalysts. From the viewpoint of microstructure, it was evident that the thiophene HDS reaction occurs primarily at the edge of CoMoS active phases and that the olefin hydrogenation reaction occurs mainly at the corner of MoS_2 active phases. The investigation not only promotes a new understanding of the nature of CoMoS and MoS_2 active phases coexisting on sulfided $CoMo/Al_2O_3$ catalysts for the selective hydrodesulfurization (HDS) of gasoline but also provides a facile method to prepare highly selective HDS catalysts by finely tuning the EDTA/Co molar ratio and the Co content on the $CoMo/Al_2O_3$ catalysts.

Acknowledgments

The authors gratefully acknowledge the financial support of the National Natural Science Foundation of China (Grant Nos. 21076228 and U1162116).

Appendix A. Supplementary data

Supplementary data associated with this article can be found, in the online version, at http://dx.doi.org/10.1016/j.apcatb.2017.08.029.

References

[1] H. Ziaei-Azad, N. Semagina, Appl. Catal. B: Environ. 191 (2016) 138–146.
[2] R. Singh, D. Kunzru, S. Sivakumar, Appl. Catal. B: Environ. 185 (2016) 163–173.
[3] S. Brunet, D. Mey, G. Pérot, C. Bouchy, F. Diehl, Appl. Catal. A Gen. 278 (2005) 143–172.
[4] C. Song, Catal. Today 86 (2003) 211–263.
[5] D. Ishutenko, A. Mozhaev, V. Salnikov, P. Nikulshin, Reaction Kinetics, Mechan. Catal. 119 (2016) 615–627.
[6] T.G. Albro, P.A. Dreifuss, R.F. Wormsbecher, J. High Res. Chromatogr. 16 (1993) 13–17.
[7] W.C. Cheng, G. Kim, A.W. Peters, X. Zhao, K. Rajagopalan, Catal. Rev.-Sci. Eng. 40 (1998) 39–79.
[8] C. Yin, G. Zhu, D. Xia, Fuel Process. Technol. 79 (2002) 135–140.
[9] L.G. Woolfolk, C. Geantet, L. Massin, D. Laurenti, J.A.D. Reyes, Appl. Catal. B: Environ. 201 (2017) 331–338.
[10] B. Liu, L. Liu, Z. Wang, Y. Chai, H. Liu, C. Yin, C. Liu, Catal. Today 282 (2017) 214–221.
[11] T. Wang, Y. Fan, X. Wang, L. Chou, H. Lin, Fuel 157 (2015) 171–176.
[12] Y. Fan, J. Lu, G. Shi, H. Liu, X. Bao, Catal. Today 125 (2007) 220–228.
[13] P. Yu, M. Ke, Q. Liu, X. Yan, J. Li, RSC Adv. 6 (2016) 96662–96668.
[14] H. Topsøe, B.S. Clausen, N.Y. Topsøe, P. Zeuthen, Stud. Surf. Sci. Catal. 53 (1989) 77–102.
[15] H. Topsøe, B.S. Clausen, R. Candia, C. Wivel, S. Mørup, J. Catal. 68 (1981) 433–452.
[16] J.T. Miller, W.J. Reagan, J.A. Kaduk, C.L. Marshall, A.J. Kropf, J. Catal. 193 (2000) 123–131.
[17] X.D. Wen, T. Zeng, B.T. Teng, F.Q. Zhang, Y.W. Li, J. Wang, H. Jiao, J. Mol. Catal. A: Chem. 249 (2006) 191–200.
[18] E.J.M. Hensen, P.J. Kooyman, Y. van der Meer, A.M. van der Kraan, V.H.J. de Beer, J.A.R. van Veen, R.A. van Santen, J. Catal. 199 (2001) 224–235.
[19] M. Li, H. Li, F. Jiang, Y. Chu, H. Nie, Catal. Today 149 (2010) 35–39.
[20] P.A. Nikulshin, D.I. Ishutenko, A.A. Mozhaev, K.I. Maslakov, A.A. Pimerzin, J. Catal. 312 (2014) 152–169.
[21] M.A. Lélias, E. Le Guludec, L. Mariey, J. van Gestel, A. Travert, L. Oliviero, F. Maugé, Catal. Today 150 (2010) 179–185.
[22] S.L. González-Cortés, T.C. Xiao, P.M.F.J. Costa, B. Fontal, M.L.H. Green, Appl. Catal. A: Gen. 270 (2004) 209–222.
[23] J. Xu, T. Huang, Y. Fan, Appl. Catal. B: Environ. 203 (2017) 839–850.
[24] Q. Gao, T.N.K. Ofosu, S.G. Ma, V.G. Komvokis, C.T. Williams, K. Segawa, Catal. Today 164 (2011) 538–543.
[25] A.M. Venezia, Catal. Today 77 (2003) 359–370.
[26] T.K.T. Ninh, L. Massin, D. Laurenti, M. Vrinat, Appl. Catal. A: Gen. 407 (2011) 29–39.
[27] P.A. Nikulshin, A.V. Mozhaev, K.I. Maslakov, A.A. Pimerzin, V.M. Kogan, Appl. Catal. B: Environ. 158–159 (2014) 161–174.
[28] Y. Fan, G. Shi, H. Liu, X. Bao, Appl. Catal. B: Environ. 91 (2009) 73–82.
[29] A. Travert, C. Dujardin, F. Maugé, E. Veilly, S. Cristol, J.F. Paul, E. Payen, J. Phys Chem B. 110 (2006) 261–270.
[30] M.A. Lélias, P.J. Kooyman, L. Mariey, L. Oliviero, A. Travert, J. van Gestel, J.A.R. van Veen, F. Maugé, J. Catal. 267 (2009) 14–23.
[31] J.S. Choi, F. Maugé, C. Pichon, J. Olivier-Fourcade, J.C. Jumas, C. Petit-Clair, D. Uzio, Appl. Catal. A Gen. 267 (2004) 203–216.
[32] D. Mey, S. Brunet, C. Canaff, F. Maugé, C. Bouchy, F. Diehl, J. Catal. 227 (2004) 436–447.
[33] C. Dujardin, M.A. Lélias, J. van Gestel, A. Travert, J.C. Duchet, F. Maugé, Appl. Catal. A Gen. 322 (2007) 46–57.

[34] A. Travert, C. Dujardin, F. Maugé, S. Cristol, J.F. Paul, E. Payen, D. Bougeard, Catal. Today 70 (2001) 255–269.
[35] F. Maugé, J.C. Lavalley, J. Catal. 137 (1992) 69–76.
[36] R. Cattaneo, T. Shido, R. Prins, J. Catal. 185 (1999) 199–212.
[37] K. Al-dalama, A. Stanislaus, Energy Fuels 20 (2006) 1777–1783.
[38] R. Cattaneo, T. Weber, T. Shido, R. Prins, J. Catal. 191 (2000) 225–236.
[39] J. Escobar, M.C. Barrera, J.A. de los Reyes, J.A. Toledo, V. Santes, J.A. Colín, J. Mol. Catal. A Chem. 287 (2008) 33–40.
[40] S.M.A.M. Bouwens, F.B.M. Vanzon, M.P. Vandijk, A.M. Vanderkraan, V.H.J. Debeer, J.A.R. Vanveen, D.C. Koningsberger, J. Catal. 146 (1994) 375–393.
[41] C. Wivel, R. Candia, B.S. Clausen, S. Mørup, H. Topsøe, J. Catal. 68 (1981) 453–463.
[42] E. Payen, R. Hubaut, S. Kasztelan, O. Poulet, J. Grimblot, J. Catal. 147 (1994) 123–132.
[43] T. Fujikawa, H. Kimura, K. Kiriyama, K. Hagiwara, Catal. Today 111 (2006) 188–193.
[44] S. Eijsbouts, L. Vandenoetelaar, R. Vanpuijenbroek, J. Catal. 229 (2005) 352–364.
[45] G. Berhault, M. Perez De la Rosa, A. Mehta, M.J. Yácaman, R.R. Chianelli, Appl. Catal. A Gen. 345 (2008) 80–88.
[46] O.Y. Gutiérrez, T. Klimova, J. Catal. 281 (2011) 50–62.
[47] B. Liu, Y. Chai, Y. Liu, Y. Wang, Y. Liu, C. Liu, Fuel 95 (2012) 457–463.
[48] D. Laurenti, B. Phung-Ngoc, C. Roukoss, E. Devers, K. Marchand, L. Massin, L. Lemaitre, C. Legens, A.A. Quoineaud, M. Vrinat, J. Catal. 297 (2013) 165–175.
[49] A.D. Gandubert, E. Krebs, C. Legens, D. Costa, D. Guillaume, P. Raybaud, Catal. Today 130 (2008) 149–159.
[50] P. Nikulshin, D. Ishutenko, Y. Anashkin, A. Mozhaev, A. Pimerzin, Fuel 182 (2016) 632–639.
[51] R. Candia, O. Sørensen, J. Villadsen, N.Y. Topsøe, B.S. Clausen, H. Topsøe, Bull. Soc. Chim. Belg. 93 (1984) 763–773.
[52] K. Inamura, R. Prins, Stud. Surf. Sci. Catal. 92 (1995) 401–412.
[53] J.S. Choi, C. Petit-Clair, D. Uzio, Stud. Surf. Sci. Catal. 143 (2002) 585–592.
[54] M. Toba, Y. Miki, Y. Kanda, T. Matsui, M. Harada, Y. Yoshimura, Catal. Today 104 (2005) 64–69.
[55] S. Hatanaka, M. Yamada, Ind. Eng. Chem. Res. 36 (1997) 5110–5117.
[56] S. Harris, R.R. Chianelli, J. Catal. 98 (1986) 17–31.
[57] E. Krebs, B. Silvi, A. Daudin, P. Raybaud, J. Catal. 260 (2008) 276–287.
[58] S. Liu, X. Liang, J. Zhang, B. Chen, Catal. Sci. Technol. 7 (2017) 466–480.